*Korean J. Chem. Eng.*, 33(1), 159-169 (2016)
DOI: 10.1007/s11814-015-0110-2

pISSN: 0256-1115
eISSN: 1975-7220

# Removal of $Pb^{2+}$ from the aqueous solution by tartrate intercalated layered double hydroxides

**Yanming Shen†, Xiaolei Zhao, Xi Zhang, Shifeng Li, Dongbin Liu, and Lihui Fan**

Department of Chemical Engineering, Shenyang University of Chemical Technology, No. 11 Street, Shenyang Economical and Development Zone, Shenyang 110142, China
(*Received 3 October 2014 • accepted 26 May 2015*)

**Abstract**−Adsorption of $Pb^{2+}$ ion by a tartrate intercalated MgAl layered double hydroxides (MgAl-TA LDHs) was studied. The adsorption isotherms and kinetics were investigated as a function of various experimental parameters using batch adsorption experiments. The results indicated that the adsorption isotherm was well described by Sips model. The kinetic adsorption data were fitted well to the pseudo-second-order kinetic equation. The adsorption of $Pb^{2+}$ was controlled mainly by the chemical process combined with intraparticle diffusion. Parameters of adsorption thermodynamic suggested that the interaction of $Pb^{2+}$ adsorbed by MgAl-TA LDHs adsorbents was thermodynamically spontaneous and endothermic.

Keywords: Layered Double Hydroxide, Hydrotalcite, Adsorption, Heavy Metal Ions

## INTRODUCTION

With the rapid development of industries such as metal plating, mining operations, fertilizer industries, tanneries, batteries, paper making and pesticides, wastewaters containing heavy metal ions are increasingly directly or indirectly discharged into the environment. Unlike organic contaminants, heavy metals are not biodegradable and tend to accumulate in living organisms, and many heavy metal ions are known to be toxic or carcinogenic [1]. Lead is one of the most abundant heavy metals in the environment. The accumulation of $Pb^{2+}$ in the human body can introduce a range of serious health afflictions, including muscle paralysis, mental confusion, memory loss, and anemia, suggesting that $Pb^{2+}$ affects multiple targets in vivo. Even worse, such pollution may persist for two millennia [2]. So far, various methods have been proposed for the efficient removal of heavy metal ions from the waters, including but not limited to coagulation, chemical precipitation, membrane filtration, reverse osmosis, solvent extraction, flotation, ion exchange and adsorption [3]. Among these, adsorption is now recognized as effective and economical for heavy metal wastewater treatment. Besides the common activated carbon adsorbents, many low-cost adsorbents such as agricultural and industrial by-products and wastes [4,5], natural substances [6,7] have been studied as adsorbents for the removal of heavy metal ions. Recently, layered double hydroxides (LDHs) were developed as the adsorbents to adsorb heavy metal ions from wastewater owing to their layer structure, good anion exchange capacity, and simple synthesis, low cost and environmental friendliness [8]. It was reported that $Pb^{2+}$ could be removed rapidly from an aqueous solution on Mg-Al-$CO_3$ LDHs with the adsorption capacity of 66.16 $mg \cdot g^{-1}$ [9]. The large removal capacity of $Pb^{2+}$ was also obtained on Ca-Al-$NO_3$ and Co-Bi-$CO_3$ LDHs [10,11]. It was stated that plenty of $OH^-$ on the surfaces of LDHs supplied the main adsorption sites, and the precipitation of a hydroxide on the surfaces was the main mechanism for $Pb^{2+}$ removal by the LDHs.

Fundamentally, a chelating agent such as EDTA has strong, selective metal binding properties, ability to form a 1 : 1 chelate with a metal ion; thus a type of chelating ion-exchange resin, which consists of two components, a chelating group and a polymeric matrix, has a better adsorption capacity for heavy metal ions [12]. Similarly, when the chelating agent anions are introduced into the interlayer space of LDHs, the LDHs adsorption capacity for heavy metal ions could be further improved, owing to the combination with the chelating [13-18]. Compared to EDTA, organic acid chelating agents such as citric, malic, and tartaric acids are inexpensive and easily biodegraded, therefore more suitable for large-scale remediation of aqueous environments [12-14]. Our previous work showed that glutamate intercalated MgAl LDHs could rapidly remove $Pb^{2+}$ from an aqueous solution with the adsorption capacity of 68.49 mg/g at 25 °C [17]. In this work, the tartrate intercalated MgAl LDHs was tested as the adsorbent to removal $Pb^{2+}$ from aqueous solutions. Some effects on the adsorption efficiency and adsorption isotherm and kinetics were investigated.

## MATERIALS AND METHODS

### 1. Materials

All the reagents were of analytical grade and purchased from the Sinopharm Chemical Reagent Company, Ltd., China. They were used without further purification.

The carbonate intercalated MgAl LDHs precursor with Mg/Al ratio of 2.0 was prepared by co-precipitation as described elsewhere

†To whom correspondence should be addressed.
E-mail: sym6821@sina.com.cn

[19]; the resultant material was labeled as MgAl-$CO_3$ LDHs. The tartrate intercalated MgAl LDHs was prepared by an anion-exchange method. Typically, 0.72 g disodium tartrate was dissolved in 100 ml ethylene glycol in a three-neck flask. The pH was adjusted in the range of 4 and 5 by adding 0.1 mol/L $HNO_3$. Then 2.0 g as-prepared MgAl-$CO_3$ LDHs was added into the above solution. The mixture was kept refluxed at 120 °C for 5 h and then cooled to room temperature. The resultant was recovered by filtering the suspension, which was followed by repeated washing with deionized water and drying at 80 °C for 12 h. The resultant was labeled as MgAl-TA LDHs.

**2. Characterization**

The phases of the resultant samples were analyzed by X-ray diffraction (XRD) using a Bruker D8 ADVANCE diffractometer under CuK$\alpha$ radiation ($\lambda$=0.15406 nm), operating at 40 KV and 40 mA over the $2\theta$ range from 3 to 75°. FT-IR spectra were recorded on a Nicolet Nexus 470 spectrometer (Thermo Nicolet Corporation, USA) under scan range 400-4,000 $cm^{-1}$ using KBr pellets (1/10 weight%). Scanning electron microscope (SEM) images were taken by a JSM-6360LV (JEOL, Japan) at 10.0 kV. The BET surface area, total pore volume, and average pore diameter of the samples were analyzed by a V-Sorb 2800P Analyser (Gold APP Instrument Corporation, China), using the multipoint $N_2$ adsorption-desorption method at liquid nitrogen temperature (−196 °C). Prior to the analyses, the samples were degassed at 120 °C and $10^{-4}$ Torr for 4 h to evacuate the physically adsorbed moisture.

**3. Batch Studies**

Lead stock solution of 1,000.0 mg/L was prepared using the $Pb(NO_3)_2$ into deionized water. The initial $Pb^{2+}$ concentration varied from 10.0 to 300.0 mg/L by diluting the stock solution.

Batch adsorption experiments were carried out in beakers by adding a certain amount of adsorbent in 100.0 mL of aqueous metal solution at desired initial pH, metal ion concentration and temperature. The initial pH was adjusted with solutions of 0.1 mol/L $HNO_3$ or 0.1 mol/L NaOH. The beakers were gently agitated in a temperature-controlled water bath at 200 rpm for a 2 h. All the experiments were performed in triplicate at the desired initial conditions and the concurrent value was taken. The content of the flask was separated from the adsorbent by filtration, using 0.42 μm micropore filter and the filtrate was analyzed for the remaining metal concentration in the sample using an atomic absorption spectrophotometer (AA-6300C, Oxford, Japan). The $Pb^{2+}$ adsorption capacities of the samples were calculated as follows:

$$\eta\% = \frac{C_0 - C_t}{C_0} \times 100\% \quad (1)$$

$$q_t = \frac{(C_0 - C_t)V}{m} \quad (2)$$

where $q_t$ (mg/g) is the amount of $Pb^{2+}$ adsorbed at adsorption time t. $C_0$ and $C_t$ (mg/L) are the concentrations of $Pb^{2+}$ in the solution at the beginning and adsorption time t, respectively. V (L) is the volume of the solution and m (g) is the weight of the adsorbent. The effects of the adsorbent dosage, the initial $Pb^{2+}$ concentration, pH and adsorption temperature on the $Pb^{2+}$ removal were investigated.

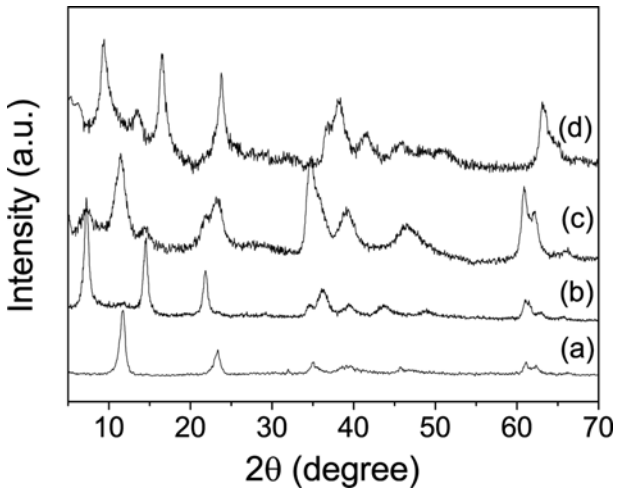


**Fig. 1. XRD patterns of (a) MgAl-$CO_3$ LDHs, (b) MgAl-TA LDHs, (c) Pb-adsorbed MgAl-TA LDHs and (d) regenerated MgAl-TA LDHs.**

## RESULTS AND DISCUSSION

**1. Characterization of MgAl-TA Adsorbent**

The XRD patterns of the precursor MgAl-$CO_3$ LDHs and the prepared MgAl-TA LDHs are shown in Fig. 1. The XRD pattern of MgAl-$CO_3$ LDHs (Fig. 1(a)) shows characteristic sharp peaks at $2\theta$=11.6°, 23.4°, 35.1°, 39.3°, 61.1° and 62.3° that are related to the hydrotalcite lattice planes of (003), (006), (009), (012), (110) and (113), respectively (JCPDS 41-1428). The MgAl-$CO_3$ LDHs precursor gives a basal spacing of 0.76 nm, which is calculated from the (003) diffraction, and the interlayer spacing is calculated of 0.28 nm by subtracting the thickness of the brucite-like layers (0.48 nm) from the basal spacing. As shown in Fig. 1(b), MgAl-TA LDHs shows a similar pattern as that of MgAl-$CO_3$ LDHs, but an obvious shift in the (003) reflection to lower angle. The interlayer spacing expands to 1.22 nm, indicating that the TA anions have been successfully

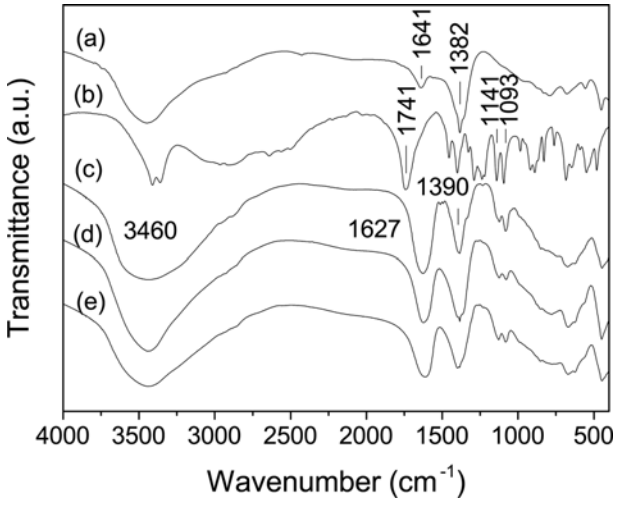


**Fig. 2. FT-IR spectra of (a) MgAl-$CO_3$ LDHs, (b) tartaric acid, (c) MgAl-TA LDHs, (d) Pb-adsorbed MgAl-TA LDHs and (e) regenerated MgAl-TA LDHs.**

intercalated into the interlayer region. By contrast, the reflection line of the diffraction peak of (110) reflection does not move, which indicates that the intercalation of the TA anions does not change the structure of the layer but only changes the interlayer spacing [20]. Moreover, there are still weak peaks at $2\theta$=11.6°, 35.1°, indicating the existence of $CO_3^{2-}$ in the interlayer space. These results are similar to that of the previous report [21], where the tartrate intercalated MgAl LDHs was prepared by the ion-exchange method.

Fig. 2 shows the FT-IR spectra of MgAl-$CO_3$ LDHs, MgAl-TA

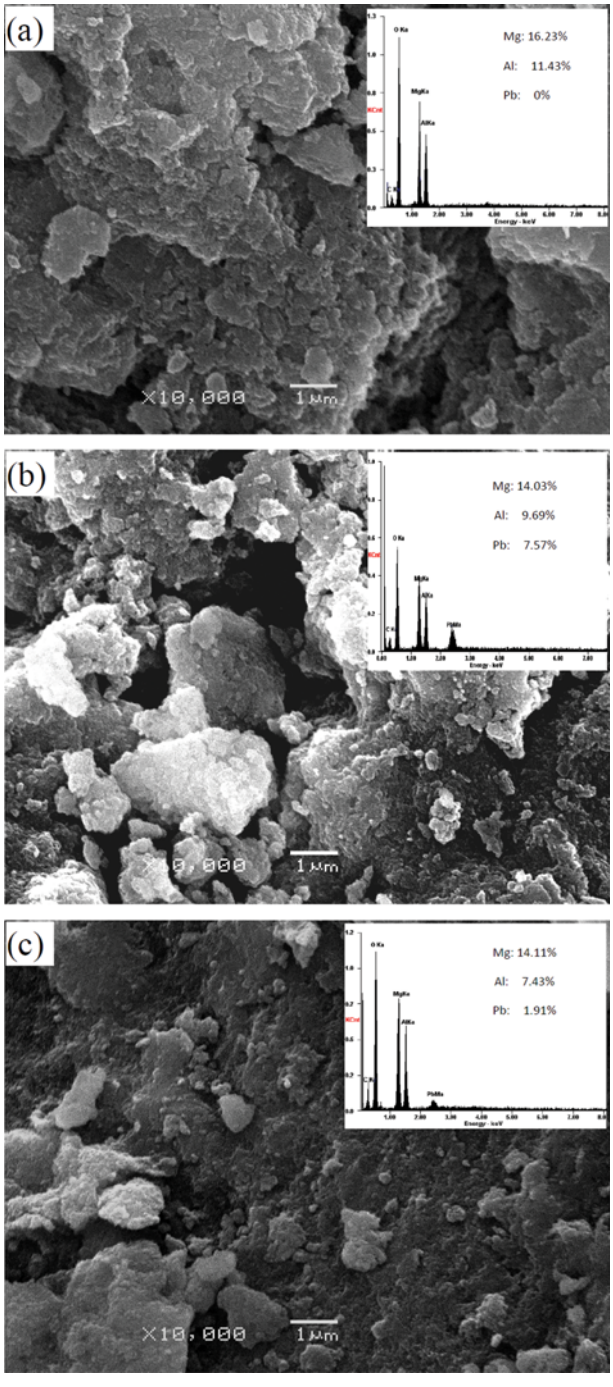


**Fig. 3. SEM images of (a) MgAl-TA LDHs, (b) Pb-adsorbed MgAl-TA LDHs and (c) regenerated MgAl-TA LDHs.**

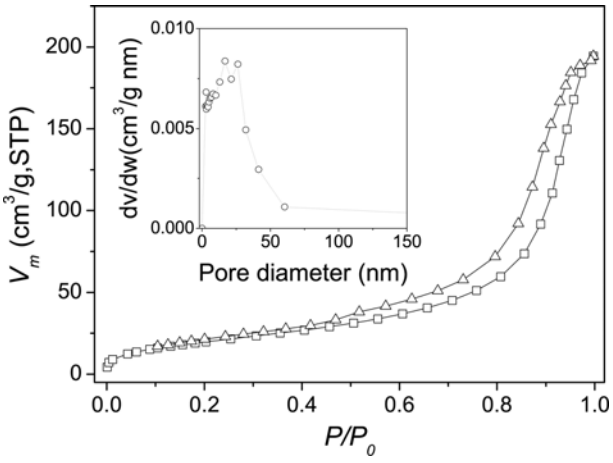


**Fig. 4. $N_2$ adsorption-desorption isotherm and the pore size distribution of MgAl-TA LDHs.**

LDHs and tartaric acid. The typical bands at 1,641 and 1,382 $cm^{-1}$ in the spectrum of MgAl-$CO_3$ LDHs are attributed to the bending vibration of $OH^-$ and the stretching vibration of carbonate [22]. The band at 1,741 $cm^{-1}$ in the spectrum of tartaric acid belongs to the carboxyl group. In the spectrum of MgAl-TA LDHs, two bands at 1,390 and 1,627 $cm^{-1}$ can be ascribed to the symmetric and asymmetric stretching vibrations of the carboxyl, respectively [22,23]. Two stretching vibrations of the alcoholic groups in tartrate centered at 1,141 and 1,093 $cm^{-1}$ also exhibit in MgAl-TA LDHs. These results show that the citrate is present in the interlayer of MgAl-TA LDHs.

The SEM image of MgAl-TA LDHs shown in Fig. 3 indicates a plate-like structure. The plate-like slabs stack up closely with each other, which is typical for LDHs.

To give the further insight on the specific area and porosity of the prepared MgAl-TA LDHs, $N_2$ adsorption measurement was carried out. Fig. 4 shows the $N_2$ adsorption-desorption isotherm and the pore size distribution curve of MgAl-TA LDHs. The sample exhibits a typical IV isotherm with a H3-type hysteresis loop, indicating the presence of mesopore [22,24]. From the pore size distribution curve (Fig. 4 inset), the distribution of pores is clearly in the range 3-50 nm. The average pore diameter and the specific area are 11.9 nm and 74.7 $m^2/g$, respectively.

**2. Effect of Adsorbent Dosage**

The effect of adsorbent dosage on the adsorption efficiency for $Pb^{2+}$ was carried out at 25 °C; the $Pb^{2+}$ concentration of 100.0 mg/L and pH of 5.0, the results are shown in Fig. 5. $Pb^{2+}$ adsorption efficiency almost approaches the equilibrium value within 30 mins, except for the adsorbent dosage of 1.0 g/L. The lower adsorption efficiency at the adsorbent dosage of 1.0 g/L is owing to the insufficient vacant adsorption sites on the surface of adsorbent. When the adsorbent dosage increases to 2.0 g/L, there are sufficient vacant adsorption sites on the surfaces; thus $Pb^{2+}$ can be rapidly adsorbed, resulting in that the adsorption efficiency increases rapidly. A further increase in the adsorbent dosage makes the increase in adsorption efficiency, but does not increase proportionally with the increase in the adsorbent dosage, owing to the reduction in overall surface area of the adsorbent probably because of aggregation during the adsorption. From Fig. 5 inset, it is indicated that the amount of

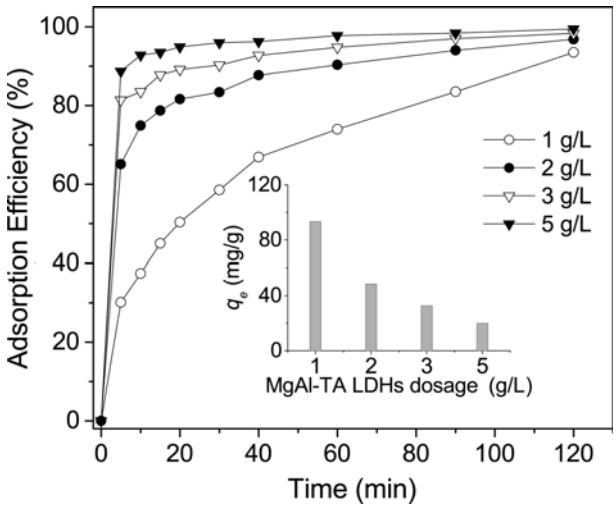


**Fig. 5. Effect of MgAl-TA adsorbent dosage on the adsorption of $Pb^{2+}$.**

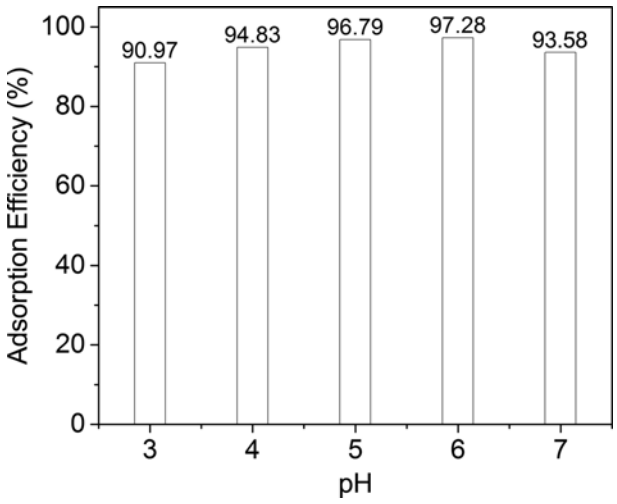


**Fig. 7. Effect of pH on the adsorption of $Pb^{2+}$.**

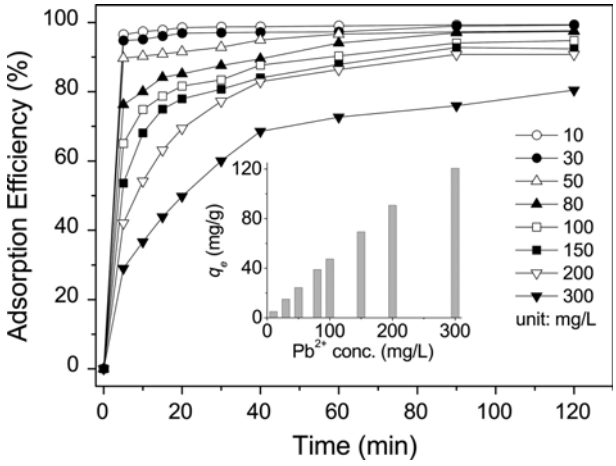


**Fig. 6. Effect of initial $Pb^{2+}$ concentration on the adsorption of $Pb^{2+}$.**

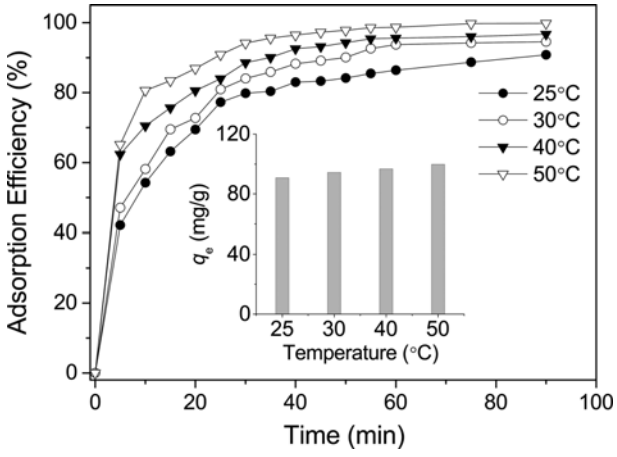


**Fig. 8. Effect of adsorption temperature on the adsorption of $Pb^{2+}$.**

$Pb^{2+}$ adsorbed on unit mass of the adsorbent at equilibrium ($q_e$) decreases with the increase in adsorbent dosage. Therefore, the adsorbent dosage of 2.0 g/L is considered the suitable value, considering the cost in practice.

**3. Effect of Initial $Pb^{2+}$ Concentration**

Fig. 6 shows the effect of initial $Pb^{2+}$ concentration on the adsorption efficiency. The results were obtained by changing the $Pb^{2+}$ concentration from 10.0 to 300.0 mg/L at 25 °C, the adsorbent dosage of 2.0 g/L and pH of 5.0. As shown in Fig. 6, the adsorption efficiency for $Pb^{2+}$ decreases with the increase in initial $Pb^{2+}$ concentration. However, the adsorbed amounts of $Pb^{2+}$ per mass of adsorbent are higher in higher initial $Pb^{2+}$ concentrations as compared to that in the lower initial $Pb^{2+}$ concentrations (see Fig. 6 inset). The $Pb^{2+}$ concentration provides an important driving force to overcome the mass transfer resistance between adsorbents and aqueous solutions. It means that at higher initial $Pb^{2+}$ concentrations, the driving force was higher than that of the lower initial $Pb^{2+}$ concentrations. Consequently, the adsorbed amounts of $Pb^{2+}$ per mass of adsorbent will be higher in case of higher initial $Pb^{2+}$ concentrations. However, at higher initial $Pb^{2+}$ concentrations the available adsorption sites become comparatively fewer, hence lowering the adsorption percentage of $Pb^{2+}$.

**4. Effect of pH**

The effect of pH on $Pb^{2+}$ adsorption on MgAl-TA LDHs is shown in Fig. 7. These results were obtained at 25 °C, $Pb^{2+}$ concentration of 100.0 mg/L and adsorbent dosage of 2.0 g/L. The adsorption efficiency increases with the increase in the pH value and reaches the maximum at pH of 5.0-6.0, then slightly decreases to a plateau at pH value of 7.0. In fact, at pH value under the zero charge point (ZCP), the surfaces are positively charged, and there exist appreciable concentrations of $H^+$ ions that compete with already present $Pb^{2+}$ ions for available binding sites, resulting in the decrease in the $Pb^{2+}$ adsorption. At the pH value above the ZCP, the surfaces are negatively charged, the number of $H^+$ ions decreases and hence more sites are available for $Pb^{2+}$ adsorption [9].

**5. Effect of Adsorption Temperature**

The effect of adsorption temperature on Fig. 8 shows the change in $Pb^{2+}$ adsorption efficiency with the adsorption temperature. These results were obtained at 25 °C, pH of 5.0, the adsorbent dosage of

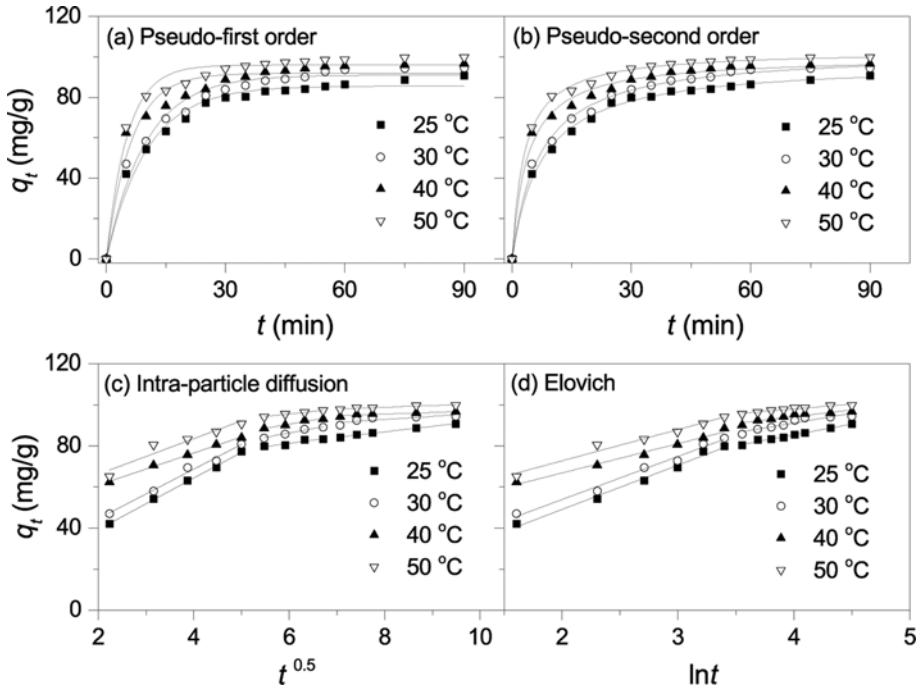


**Fig. 9. Kinetics fitting curves for adsorption of $Pb^{2+}$ at different temperatures.**

**Table 1. Parameters of adsorption kinetics for $Pb^{2+}$ on MgAl-TA LDHs adsorbent at different temperatures**

| Temperature (°C) | Pseudo-first order | | | | Pseudo-second order | | | |
|---|---|---|---|---|---|---|---|---|
| | $q_{e1}$ | $k_1$ | $R^2$ | Δq (%) | $q_{e2}$ | $k_2\times10^3$ | $R^2$ | Δq (%) |
| 25 | 85.6 | 0.09806 | 0.9793 | 6.37 | 97.4 | 1.39 | 0.9963 | 2.48 |
| 30 | 90.9 | 0.1014 | 0.9735 | 7.02 | 102.9 | 1.61 | 0.9949 | 4.17 |
| 40 | 91.9 | 0.1603 | 0.9510 | 7.15 | 100.2 | 2.60 | 0.9895 | 3.40 |
| 50 | 95.9 | 0.1910 | 0.9755 | 4.64 | 103.3 | 3.16 | 0.9976 | 1.43 |

2.0 g/L and $Pb^{2+}$ concentration of 200.0 mg/L. The adsorption efficiency increases by increasing the adsorption temperature, indicating that the adsorption process is the endothermic process.

**6. Adsorption Kinetics**

Adsorption kinetics is generally controlled by different mechanisms. Usually, pseudo-first order, pseudo-second order, intra-particle diffusion and Elovich kinetics models were applied to fit the experimental data [25].

Pseudo-first-order equation can be expressed as:

$$q_t = q_e(1-e^{-k_1 t}) \tag{3}$$

where $q_e$ and $q_t$ are the amounts of $Pb^{2+}$ adsorbed at equilibrium and at time t (mg/g), respectively. $k_1$ ($min^{-1}$) is the rate constant of pseudo-first order adsorption.

Pseudo-second-order equation is described as:

$$q_t = \frac{k_2 q_e^2 t}{1+k_2 q_e t} \tag{4}$$

where $k_2$ is the rate constant of pseudo-second order adsorption, g/(mg·min). The fitting curves are shown in Fig. 9 and the calculated kinetic constants for pseudo-first and pseudo-second order models are listed in Table 1. To evaluate the fitting model, the normalized standard deviation (Δq%) is used for comparison defined by [26]:

$$\Delta q(\%) = 100\times\sqrt{\frac{\sum[(q_{t,exp}-q_{t,cal})/q_{t,exp}]^2}{N-1}} \tag{5}$$

where the subscripts exp and cal denote the experimental and calculated values, respectively, and N is the number of data points. The determination coefficients $R^2$ and the normalized standard deviation Δq(%) listed in Table 1 indicate that the experimental data are in good agreement with the pseudo-second-order model, which suggests that the rate-limiting step in adsorption is controlled by chemical process [27].

The intra-particle diffusion equation describes the movement of ions from the bulk solution to the solid phase. This kinetics equation is expressed as [28]:

$$q_t = k_3 t^{0.5} + C \tag{6}$$

where $k_3$ is the intraparticle diffusion rate constant, mg/(g·$min^{0.5}$), C is the intercept. By using this model, the plot of $q_t$ versus $t^{0.5}$ should be linear if the intraparticle diffusion is involved in the adsorption process, and if these lines pass through the origin then the intra-

particle diffusion is the rate-controlling step. As shown in Fig. 9(c), the plots of $q_t$ vs. $t^{0.5}$ for $Pb^{2+}$ are shown in three stages. The first sharper portion is the external surface adsorption or instantaneous adsorption stage. The second portion is the gradual adsorption stage, where the intra-particle diffusion is rate-controlled. The third portion is the final equilibrium stage, where the intraparticle diffusion starts to slow down due to the extremely low solute concentration in solution [29]. The strong linear correlation indicates that intra-particle diffusion is involved in the adsorption process, but the non-zero intercept suggests that it is not the rate-controlling step [30].

The Elovich equation interprets the predominantly chemical adsorption on highly heterogeneous adsorbents. The Elovich equation can be described as:

$$q_t=\beta \ln(\alpha\beta)+\beta \ln t \tag{7}$$

The coefficient $\alpha$ is the initial adsorption rate [g/(mg $min^2$)] and $\beta$ is the desorption constant [mg/(g min)] related to the extent of surface coverage and activation energy for chemisorption. As described in Fig. 9(d), the plots of $q_t$ vs. ln(t) display a relatively good linear relationship before reaching the adsorption equilibrium. This result shows the heterogeneous distribution of the adsorption energy in the adsorption process [28].

In summary, the adsorption kinetics were well fitted by a pseudo-second-order kinetic model, showing the adsorption process was controlled by the chemical process, but the intra-particle diffusion could not be ignored during the adsorption process.

**7. Adsorption Isotherm**

An adsorption isotherm represents the amount of species adsorbed versus the amount of species left in the solution phase at equilibrium. The adsorption data were analyzed by Langmuir, Freundlich, Temkin, Redlich-Peterson and Sips isotherms. The association of fitness of the model prediction with experimental data requires an error function with optimization. Along with the coefficient of determination ($R^2$), the residual root mean square error (RMSE) and the chi-square test ($\chi^2$) were also calculated to measure the goodness of fit [31]. RMSE and $\chi^2$ can be defined as:

$$\mathrm{RMSE}=\sqrt{\frac{1}{N-1}\sum_{i=1}^{N}(q_{e,\,exp}-q_{e,\,cal})^2} \tag{8}$$

$$\chi^2=\sum_{i=1}^{N}\frac{(q_{e,\,exp}-q_{e,\,cal})^2}{q_{e,\,exp}} \tag{9}$$

where $q_{e,exp}$ is the equilibrium adsorption capacity found from the batch experiment, $q_{e,cal}$ is the prediction from the isotherm model for corresponding to $C_e$ and N is the number of observations in the experimental isotherm. The smaller RMSE and $\chi^2$ value indicates the better model fitting and the better similarity of the model to the experimental data.

The Langmuir model describes quantitatively the formation of a monolayer adsorbate on the outer surface of the adsorbent, and after that no further adsorption takes place. The Langmuir represents the equilibrium distribution of adsorbate between the solid and liquid phases, its equation is expressed as:

$$q_e=\frac{q_{max}K_LC_e}{1+K_LC_e} \tag{10}$$

where $q_e$ is the amount of $Pb^{2+}$ adsorbed on the adsorbent at equi-

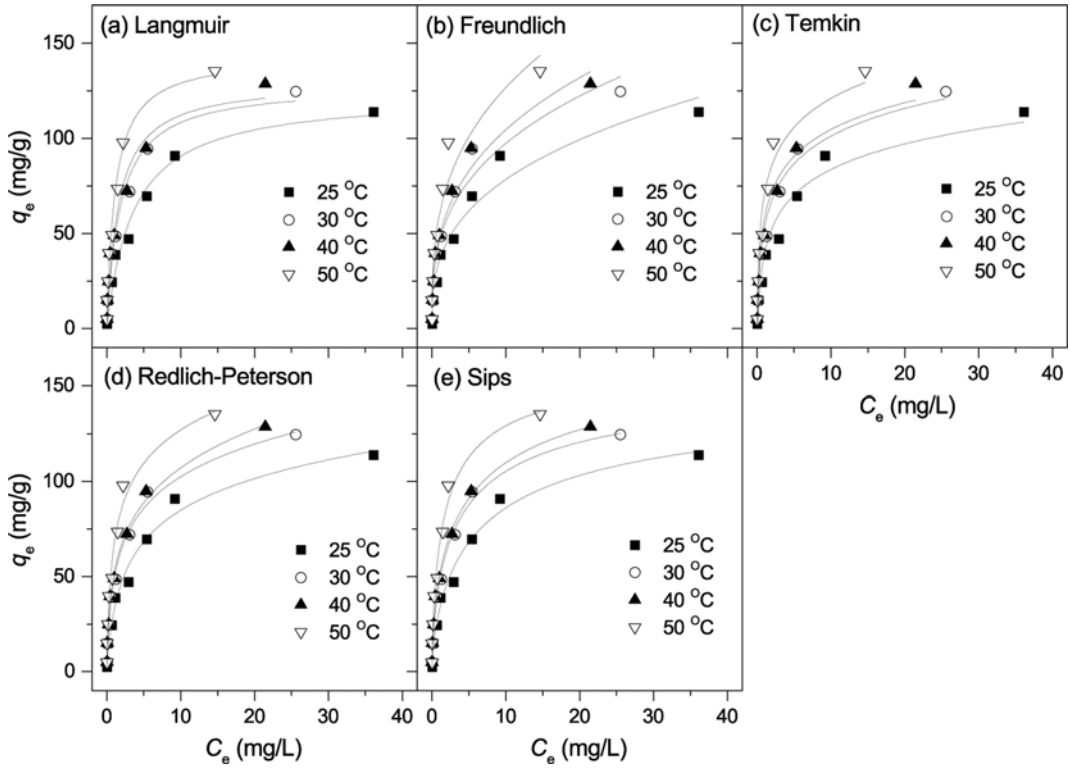


**Fig. 10. Adsorption Isotherms of $Pb^{2+}$ on MgAl-TA adsorbent at different temperatures.**

librium (mg/g), $q_{max}$ denotes the maximum adsorption capacity corresponding to complete monolayer coverage, $C_e$ describes the equilibrium $Pb^{2+}$ concentration (mg/L), and $K_L$ is the Langmuir adsorption constant (L/mg).

The Freundlich equilibrium isotherm equation is an empirical equation used for the description of multilayer adsorption with interaction between adsorbed molecules:

$$q_e=K_F C_e^{1/n} \quad (11)$$

where $K_F$ and n are the Freundlich constants related to the maximum adsorption capacity (mg/g) and the heterogeneity factor ($mg^{-1}$), respectively. The model is applicable to the adsorption on heterogeneous surfaces by a uniform energy distribution and reversible adsorption. The Freundlich equation implies that adsorption energy exponentially decreases on the finishing point of adsorptional centers of an adsorbent [47]. The Freundlich constants are empirical constants depending on many environmental factors. The value of 1/n ranges between 0 and 1, indicating the degree of non-linearity between solution concentration and adsorption.

Temkin model is based on the assumption that the heat of adsorption would decrease linearly with the increase of coverage of adsorbent and can be described as:

$$q_e=A \ln(BC_e) \quad (12)$$

where B is a constant related to the heat of adsorption (J/mol) and equals to RT/b. A is the Temkin equilibrium constant.

The Langmuir, Freundlich and Temkin fitting curves are presented in Fig. 10 and the calculated results are listed in Table 2. The Langmuir, Freundlich and Temkin model do not fit well with the experimental data, owing to the larger values of RMSE and $\chi^2$, though the relative higher value of $R^2$ (>0.92). These results suggest that the adsorption of $Pb^{2+}$ on MgAl-TA LDHs is not simply described by these models. In fact, the Langmuir model is based on the hypothesis that the surface is completely uniform and energetically homogeneous [32]. For MgAl-TA LDHs adsorbent, besides the adsorbing sites on the surface, the tartrate anions located in the interlayer space can also adsorb $Pb^{2+}$ by chelating, resulting in the surface heterogeneity of adsorbent and no better fitting results obtained by Langmuir isotherm. Both Freundlich and Temkin models revise the hypothesis for uniform surface in the Langmuir model by assuming the adsorption energy exponentially and linearly decreases on the finishing point of adsorptional centers of an adsorbent, respectively [32], but they do not give a better fitting result for the experimental data.

Redlich-Peterson model and Sips model combine the features of both the Langmuir and Freundlich isotherms into a single equation. Redlich-Peterson model is presented as follows:

$$q_e=\frac{K_{RP}C_e}{1+a_{RP}C_e^{\beta}} \quad (13)$$

In Redlich-Peterson equation, $K_{RP}$ (L/g) and $a_{RP}$ $(L/mg)^{\beta}$ are the Redlich-Peterson isotherm constants, while $\beta$ is the Redlich-Peterson isotherm exponent, which should be $0<\beta<1$. For $\beta=1$, the Redlich-Peterson model converts to the Langmuir model, while $\beta$=zero, it becomes Henry's law. Redlich-Peterson model approaches the Freundlich model at high concentration and is in accord with the low concentration limit of the Langmuir equation [33].

By identifying the problem of continuing increase in the adsorbed amount with an increase in concentration in the Freundlich equation, Sips proposed an equation similar in form to the Freundlich equation, but it has a finite limit when the concentration is sufficiently high:

$$q_e=\frac{q_m K_s C_e^m}{1+K_s C_e^m} \quad (14)$$

where $q_m$ is the Sips maximum adsorption capacity (mg/g), $K_s$ is the Sips equilibrium constant $(L/mg)^m$, and m is the Sips model exponent, limited from 0 to 1. At the low adsorbate concentrations the Sips isotherm model effectively reduces to the Freundlich isotherm and thus does not obey Henry's law. And at high adsorbate concentrations, this model predicts a monolayer adsorption capacity characteristic of the Langmuir isotherm.

The Redlich-Peterson and Sips fitting curves are shown in Fig. 10 and the fitting results are listed in Table 2. From Table 2 both

**Table 2. Parameters of adsorption isotherms for $Pb^{2+}$ on MgAl-TA LDHs adsorbent at different temperatures**

| Temp. (°C) | 25 | 30 | 40 | 50 |
|---|---|---|---|---|
| Langmuir | | | | |
| $q_{max}$ | 123.3 | 128.2 | 130.1 | 143.6 |
| $K_L$ | 0.2760 | 0.5431 | 0.6226 | 0.8822 |
| $R^2$ | 0.9675 | 0.9702 | 0.9602 | 0.9700 |
| RMSE | 6.44 | 6.61 | 7.83 | 7.15 |
| $\chi^2$ | 12.48 | 10.98 | 14.11 | 13.27 |
| Freundlich | | | | |
| $K_F$ | 35.7 | 45.7 | 48.2 | 59.4 |
| n | 2.93 | 3.05 | 2.97 | 3.04 |
| $R^2$ | 0.9508 | 0.9524 | 0.9692 | 0.9337 |
| RMSE | 7.92 | 8.34 | 6.88 | 10.63 |
| $\chi^2$ | 24.95 | 27.17 | 34.32 | 40.67 |
| Temkin | | | | |
| A | 7.5 | 12.3 | 17.2 | 24.8 |
| B | 19.4 | 21.0 | 20.3 | 21.9 |
| $R^2$ | 0.9238 | 0.9716 | 0.9499 | 0.9369 |
| RMSE | 8.42 | 5.62 | 7.67 | 9.11 |
| $\chi^2$ | 17.30 | 6.88 | 15.86 | 18.83 |
| Redlich-Peterson | | | | |
| $K_{RP}$ | 63.8 | 147.6 | 227.7 | 227.2 |
| $a_{RP}$ | 0.9679 | 2.0284 | 3.3857 | 2.3929 |
| $\beta$ | 0.8282 | 0.8204 | 0.7769 | 0.8486 |
| $R^2$ | 0.9726 | 0.9896 | 0.9921 | 0.9759 |
| RMSE | 5.40 | 3.57 | 3.19 | 5.85 |
| $\chi^2$ | 6.47 | 1.76 | 2.45 | 5.81 |
| Sips | | | | |
| $q_m$ | 153.5 | 160.4 | 184.0 | 166.8 |
| $K_s$ | 0.2656 | 0.4131 | 0.3749 | 0.6536 |
| m | 0.6820 | 0.6649 | 0.5965 | 0.7208 |
| $R^2$ | 0.9803 | 0.9934 | 0.9941 | 0.9821 |
| RMSE | 3.77 | 2.28 | 2.47 | 4.41 |
| $\chi^2$ | 2.59 | 0.74 | 2.13 | 4.38 |

**Table 3. Thermodynamics parameters for $Pb^{2+}$ on MgAl-TA LDHs adsorbent**

| $\Delta G^0$ (KJ/mol) | | | | $\Delta H^0$ | $\Delta S^0$ | $E_a$ |
|---|---|---|---|---|---|---|
| 25 °C | 30 °C | 40 °C | 50 °C | (KJ/mol) | [J/(mol·K)] | (KJ/mol)[a] |
| −29.1 | −30.1 | −32.1 | −34.1 | 30.7 | 200.6 | 27.7 |

[a]The activation energy $E_a$ calculated according to the peseudo-second-order kinetics model

Redlich-Peterson and Sips fitting curves are more suitable than Langmuir, Freundlich and Temkin fitting curves due to higher values of $R^2$ and small RMSE and $\chi^2$. By further comparing on $R^2$, RMSE and $\chi^2$, Sips model appears to be more suitable than Redlich-Peterson model. These results suggest the heterogeneity of surfaces on the MgAl-TA LDHs adsorbent.

**8. Adsorption Thermodynamic Parameters**

Thermodynamic parameters for adsorption of $Pb^{2+}$ onto MgAl-TA LDHs adsorbent are evaluated using the following equations [34]:

$$\Delta G^0 = -RT \cdot \ln k^0 \quad (15)$$

$$\Delta G^0 = \Delta H^0 - T\Delta S^0 \quad (16)$$

$$\ln k_c = \frac{\Delta S^0}{R} - \frac{\Delta H^0}{RT} \quad (17)$$

where, R is the universal gas constant [8.314 J/(mol·K)], T is the temperature (K), $\Delta G^0$ is the change in free energy, $\Delta H^0$ is the standard enthalpy and $\Delta S^0$ is the standard entropy, $K^0$ is the thermodynamic equilibrium constant. The Value of $K^0$ can be obtained by plotting $\ln(q_e/C_e)$ versus $q_e$ and extrapolating $q_e$ to zero [9,35]. Values of $\ln K^0$ are obtained as 11.6 (25 °C), 12.1 (30 °C), 12.3 (40 °C) and 12.7 (50 °C), respectively. $\Delta H^0$ and $\Delta S^0$ can be calculated, respectively, from the slope and intercept of plot of $\ln K_c$ vs. 1/T. The values obtained from Eqs. (15)-(17) are listed in Table 3.

As listed in Table 3, the positive value of the standard enthalpy ($\Delta H^0$) change shows that the adsorption is endothermic, which follows the result observed from the effect of temperature. The reason may be explained that, at a higher temperature, an increase in active sites occurs owing to bond rupture of functional groups on the adsorbent surface [9,36]. The negative value of $\Delta G^0$ indicates the thermodynamic spontaneous nature of adsorption process, and it is more negative at higher temperature, which indicates that the adsorption was favored by higher temperatures [37,38]. The positive value of adsorption entropy ($\Delta S^0$) shows the affinity of MgAl-TA LDH for $Pb^{2+}$ and the increased disorder at the solid/liquid interface during the adsorption process [37,38]. The activation energy $E_a$ calculated according to the pseudo-second-order kinetics model is 27.7 KJ/mol, suggesting that the adsorption process is belonged to the chemical process.

**9. Adsorbent Regeneration**

The effective reuse of adsorbent material directly affects the cost factor and hence its utility in continuous batch adsorption processes. In this work, the regeneration of the used MgAl-TA adsorbent was investigated. The Pb-adsorbed adsorbent was immersed into 1.0 mol/L sodium acetate solution for 12 h at room temperature. The pH of the immersing solution was kept in the range of 6.0 and 6.5 by the adding 0.1 mol/L acetic acid. After separation from the solution, the solid adsorbent was re-exchanged with TA solution, forming the MgAl-TA adsorbent. The $Pb^{2+}$ removal efficiency on regenerated MgAl-TA adsorbent is shown in Fig. 11. The $Pb^{2+}$ adsorption efficiencies were found to be 96.8%, 93.1% and 82.3%, respectively, for the as-prepared, 1st and 2nd regenerated adsorbent, showing the better re-use performance of MgAl-TA adsorbent.

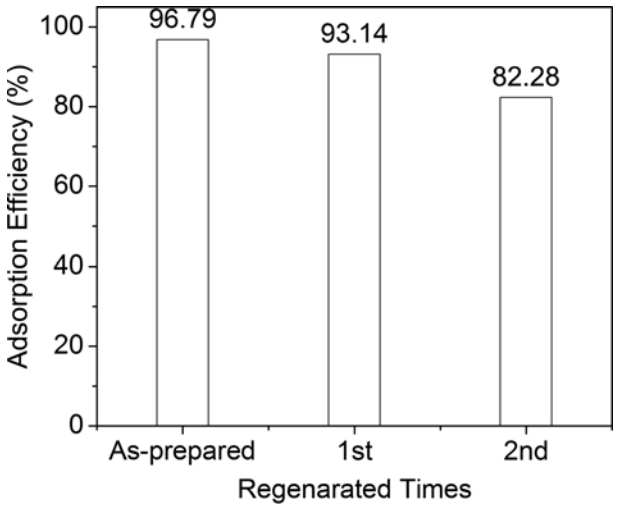


**Fig. 11. Adsorption efficiencies of $Pb^{2+}$ on as-prepared, 1st and 2nd regenerated MgAl-TA LDHs adsorbent.**

The XRD patterns of the Pb-adsorbed and regenerated adsorbents are shown in Fig. 1. The Pb-adsorbed sample exhibits the combined features of those of MgAl-$CO_3$ and MgAl-TA LDHs, showing that during the adsorption $CO_3^{2-}$ was intercalated into the interlayers, being attributed to the suspension adsorbing $CO_2$ from the atmosphere to form $CO_3^{2-}$ in the $Pb^{2+}$ adsorption process. After adsorption the slight difference in the position of the plane (110) at the diffraction angle of about 60° shows that the slight change in arrangement of metal ions in the layer, keeping the layer structure. After regeneration Pb-adsorbed MgAl-TA LDHs lost most $CO_3^{2-}$ located in the interlayer and rebuilt nearly to the origin structure of as-prepared MgAl-TA LDHs. FT-IR spectra (see Fig. 2(d) and 2(e)) show that Pb-adsorbed MgAl-TA LDHs exhibits only slight changes in the position of the asymmetric vibration of coordinated -COO- groups, which was sensitive to interactions between molecules. It could be an indication of chelating of the metals with the interlayer ligands [39]. This band moves to lower wavenumber after adsorption, indicating the coordination between $Pb^{2+}$ and -COO- groups. After regeneration, this band moves nearly to the same position as that of the as-prepared MgAl-TA LDHs, showing the loss of $Pb^{2+}$ from the complex. It is also observed that the intensity of the band at 1,390 $cm^{-1}$ corresponding to the symmetric vibration of -COO- groups increases after adsorption, owing to the increase in the amount of $CO_3^{2-}$ whose band located at 1,382 $cm^{-1}$, combining with the band of symmetric vibration of -COO- groups. The intensity of the vibrating band of $OH^-$ at about 3,460 $cm^{-1}$ increases and the position of this band moves to lower wavenumber, showing the increase in connection between $OH^-$ and some groups. After

**Table 4. Comparison of $Pb^{2+}$ adsorption capacities of MgAl-TA LDHs with other adsorbents**

| Adsorbents | $q_{max}$ (mg/g) | Adsorption condition | | Reference |
|---|---|---|---|---|
| | pH | Temp. | | |
| Ash | 6.0 | 25 | 588.24 | [41] |
| Hide waste | -- | 20 | 22.22 | [42] |
| Coffee residue | 5.9 | 25 | 63.29 | [43] |
| $H_2O_2$-oxidized activated carbon | 5.0 | 30 | 37.92 | [44] |
| Montmorillonite-illite type of clay | 4.0 | 30 | 51.80 | [45] |
| MgAl-$CO_3$ LDH | 5.7 | 30 | 66.16 | [9] |
| Glutamate intercalated MgAl LDHs | 5.0 | 25 | 68.49 | [17] |
| MgAl-TA LDHs[a] | <6.0 | Room temp. | 8.4 | [46] |
| MgAl-TA LDHs[b] | 5-6 | 25 | 114.3 | This work |

[a]Mg/Al=4.0
[b]Mg/Al=2.0

regeneration, the intensity and position of this band restore nearly to the origin state of as-prepared MgAl-TA adsorbent. SEM images (see Fig. 3(b) and 3(c)) indicate that Pb-adsorbed and regenerated MgAl-TA LDHs also present a plate-like morphology. EDX results show that after regeneration most Pb was removed from the adsorbent.

**10. Adsorption Mechanism**

Generally, heavy metal ions may be removed by LDHs via (i) precipitation of metal hydroxides onto the surface of LDHs; (ii) adsorption through the bonding with surface hydroxyl groups of LDHs; (iii) isomorphic substitution and (iv) chelation with the functional ligand in the interlayers [8].

Firstly, XRD results reveal that no new bulk phase is detected in the Pb-adsorbed MgAl-TA LDHs; thus precipitation should not exist during the adsorption. Secondly, the diffusion of $Pb^{2+}$ into the lattice structure of the LDHs is not basically possible, because of the steric hindrance for isomorphic substitution caused by the larger radium of $Pb^{2+}$ (0.119 nm) [8]. It is also identified by the result that there was almost no change of the lattice parameters between the as-prepared and Pb-adsorbed MgAl-TA LDHs. Thirdly, LDHs surface has some deprotonated hydroxyl groups (Sur-O-) which may form functional groups to adsorb the metal ions by forming inner-sphere surface complexes. This chemical binding adsorption process can be described as [40]:

$$Sur\text{-}OH+Pb^{2+}\rightarrow Sur\text{-}O\text{-}Pb^{+}+H^{+} \quad (18)$$

This complexation reaction is chemical binding adsorption and pH-dependent one which is identified by the results observed from the effect of pH on the adsorption (see Fig. 7). Also, this effect is not so significant that the adsorption efficiency changes a little, showing this complexation reaction is not the main adsorption process. Fourthly, the smaller ionic diameter of $Pb^{2+}$ than the mean pore diameter of the LDH (the average value is 11.95 nm) allows $Pb^{2+}$ to diffuse into the pore space of the LDHs and react with the tartrate to form Pb-tartrate chelates. This should be the main adsorption reaction during the $Pb^{2+}$ adsorption on MgAl-TA LDHs. Because, when the tartrate was introduced into the interlayer again, the regenerated adsorbent could keep the higher adsorption efficiency as as-prepared one.

On the whole, the removal of $Pb^{2+}$ cations by the MgAl-TA LDHs adsorbent is attributable largely to the formation of chelate complex between $Pb^{2+}$ and the intercalated and adsorbed tartrate. A surface complexation reaction also happens during the adsorption process.

**11. Comparison of Adsorption Capacity**

The comparison of MgAl-TA LDHs adsorbent with other adsorbents is listed in Table 4. The MgAl-TA LDHs adsorbent reported in this work has better adsorption capacity than some bioadsorbents, activated carbon and Montmorillonite type of clay, even better than other LDHs adsorbents with a similar layered structure, but lower than ash. The higher adsorption capacity of ash could be originating from the larger specific surface area.

It was reported that removal of $Pb^{2+}$ from aqueous solution by MgAl-$CO_3$ LDHs with the maximum adsorption amounts of 66.16 mg/g at 30 °C, and the adsorption isotherm can be described by Langmuir model, indicating that the binding energy on the whole surface of $Mg_2Al$-$CO_3$ LDHs is uniform [9]. For MgAl-TA LDHs adsorbent, there appear to exhibit two types of adsorbing sites: one is on the surfaces, the other is located in the intercalated tartrates. For comparison with the above value, the adsorbed amount obtained from $q_e$~$C_e$ curve is estimated as 124 mg/g at 30 °C, higher than the reported values. The significant improvement in the adsorption capacity may be owing to the contribution of chelating sites provided by tartrates that intercalated between the layers of LDHs. Also, when the intercalated anion was glutamate, the adsorption capacity was also improved, but lower than that of MgAl-TA LDHs. The reason may be attributed to the lower chelating ability of glutamate than tartrate anion.

However, our result is different from that reported on the removal of $Pb^{2+}$ with the similar material, on which the maximum adsorption amount is 8.4 mg/g at room temperature [46]. The adsorption capacity of an adsorbent is influenced by many factors, such as the specific surface area, pore structure, the amount of adsorption site, adsorption conditions, and so on. The following reasons may explain the different result obtained by Yasin's and our work. One reason may be the different $Mg^{2+}/Al^{3+}$ molar ratio in the prepared tartrate intercalated MgAl LDHs adsorbents. In Yasin's report, the $Mg^{2+}/Al^{3+}$ molar ratio is 4, twice that of our work. The larger

the number of $Mg^{2+}$ ions in the layers of LDHs, the smaller the number of excess positive charges in the layers; as a result, a small number of tartrate anions will be needed to intercalate into the interlayer space to keep the neutrality of the MgAl-TA LDHs [47]. Thus, the adsorption capacity reported by Yasin et al. is lower than that of our work. The second possible reason is the different structure parameters of MgAl-TA LDHs obtained in Yasin's and our work, owing to different preparation methods used. In Yasin's work, MgAl-TA LDHs was prepared by co-precipitation, while by ion-exchange method in our work. Also, the crystallinity of MgAl-TA LDHs prepared in Yasin's work was rather poorer than that of MgAl-TA LDHs prepared in our work. The poor crystallinity led to different structure parameters such as the specific surface area and pore distribution. Though these structure parameters were not provided in Yasin's report, one can deduce that the structural parameters of MgAl-TA LDHs prepared in our work are more suitable to the adsorption of $Pb^{2+}$.

## CONCLUSIONS

The adsorption of $Pb^{2+}$ on tartrate intercalated MgAl layered double hydroxides was studied and some influence factors such as initial $Pb^{2+}$ concentration, adsorbent dosage, solution pH and adsorption temperature were investigated. It was shown that $Pb^{2+}$ could be rapidly absorbed to the equilibrium values within 10 min. With the increase in MgAl-TA LDHs dosage, the adsorption efficiency increased, but the amount of $Pb^{2+}$ adsorbed on unit weight adsorbent decreased. A suitable MgAl-TA LDHs adsorbent may be about 2.0 g/L. The higher the initial $Pb^{2+}$ concentration, the lower the adsorption efficiency, but the higher in per mass adsorbed amount. The adsorption efficiency increased with the increase in pH value and then reduced to a plateau; a suitable pH value is about 5.0-6.0. The adsorption isotherm data were well fitted by Sips isotherm, predicting the heterogeneous surfaces of MgAl-TA LDHs adsorbent. The adsorption kinetics data were well described by a pseudo-second-order kinetic model, showing the adsorption process was controlled by the chemical process, but the intra-particle diffusion could not be ignored. The results of adsorption thermodynamic suggested that the interaction of $Pb^{2+}$ adsorbed by MgAl-TA adsorbents was thermodynamically spontaneous and endothermic. The tartrate intercalated MgAl-LDHs has potential application in removal of $Pb^{2+}$ from aqueous solution with higher adsorption capacity.

## REFERENCES


1. F. Fu and Q. Wang, *J. Environ. Manage.*, **92**, 407 (2011).
2. Z. Zhu and W. Li, *J. Environ. Chem. Eng.*, **1**, 838 (2013).
3. W.-W. Tang, G.-M. Zeng, J.-L. Gong, J. Liang, P. Xu, C. Zhang and B.-B. Huang, *Sci. Total Environ.*, **468**, 1014 (2014).
4. K. Vijayaraghavan and U. M. Joshi, *Environ. Eng. Sci.*, **30**, 67 (2013).
5. M. Harja, G. Buema, D.-M. Sutiman, C. Munteanu and D. Bucur, *Korean J. Chem. Eng.*, **29**, 1735 (2012).
6. A. Sdiri, T. Higashi, F. Jamoussi and S. Bouaziz, *J. Environ. Manage.*, **93**, 245 (2012).
7. A. Ghaemi, M. Torab-Mostaedi, S. Shahhosseini and M. Asadollahzadeh, *Korean J. Chem. Eng.*, **30**, 172 (2013).
8. X. Liang, Y. Zang, Y. Xu, X. Tan, W. Hou, L. Wang and Y. Sun, *Colloids Surf., A*, **433**, 122 (2013).
9. D. Zhao, G. Sheng, J. Hu, C. Chen and X. Wang, *Chem. Eng. J.*, **171**, 167 (2011).
10. R. Rojas, *Appl. Clay Sci.*, **87**, 254 (2014).
11. A. Jaiswal and M. C. Chattopadhyaya, *Arab. J. Chem.* (2013), DOI: 10.1016/j.arabjc.2013.09.010.
12. J. Jachuła, D. Kołodyńska and Z. Hubicki, *Chem. Eng. Res. Des.*, **90**, 1671 (2012).
13. T. Kameda, H. Takeuchi and T. Yoshioka, *Mater. Res. Bull.*, **44**, 840 (2009).
14. T. Kameda, H. Takeuchi and T. Yoshioka, *Sep. Purif. Technol.*, **62**, 330 (2008).
15. I. Pavlovic, M. R. Pérez, C. Barriga and M. A. Ulibarri, *Appl. Clay Sci.*, **43**, 125 (2009).
16. M. R. Pérez, I. Pavlovic, C. Barriga, J. Cornejo, M. C. Hermosín and M. A. Ulibarri, *Appl. Clay Sci.*, **32**, 245 (2006).
17. Y. Shen, D. Liu, S. Li, L. Fan, S. Chen and H. Md Atiqul, *Arab. J. Chem.* (2013), DOI:10.1016/j.arabjc.2013.08.005.
18. T. Kameda, S. Saito and Y. Umetsu, *Sep. Purif. Technol.*, **47**, 20 (2005).
19. S. J. Santosa, E. S. Kunarti and Karmanto, *Appl. Surf. Sci.*, **254**, 7612 (2008).
20. F. Jiao, H. Song, W. Yang, X. Jiang, X. Chen and J. Yu, *Appl. Clay Sci.*, **75**, 92 (2013).
21. W. Zhang, J. He and C. Guo, *Appl. Clay Sci.*, **39**, 166 (2008).
22. J. Zhang, F. Zhang, L. Ren, D. G. Evans and X. Duan, *Mater. Chem. Phys.*, **85**, 207 (2004).
23. X. Zhang, L. Ji, J. Wang, R. Li, Q. Liu, M. Zhang and L. Liu, *Colloids Surf., A*, **414**, 220 (2012).
24. J. Das, D. Das and K. M. Parida, *J. Colloid Interface Sci.*, **301**, 569 (2006).
25. M. Kavand, T. Kaghazchi and M. Soleimani, *Korean J. Chem. Eng.*, **31**, 692 (2014).
26. R.-L. Tseng, F.-C. Wu and R.-S. Juang, *J. Taiwan Inst. Chem. E.*, **41**, 661 (2010).
27. Y. Liu, M. Chen and H. Yongmei, *Chem. Eng. J.*, **218**, 46 (2013).
28. S. Sen Gupta and K. G. Bhattacharyya, *Adv. Colloid Interface Sci.*, **162**, 39 (2011).
29. S. J. Allen, G. McKay and K. Y. H. Khader, *Environ. Pollut.*, **56**, 39 (1989).
30. H. Znad and Z. Frangeskides, *Desalin. Water Treat.*, **52**, 1560 (2013).
31. M. A. Hossain, H. H. Ngo, W. S. Guo and T. V. Nguyen, *Bioresour. Technol.*, **113**, 97 (2012).
32. S. Rangabhashiyam, N. Anu, M. S. Giri Nandagopal and N. Selvaraju, *J. Environ. Chem. Eng.*, **2**, 398 (2014).
33. P. Senthil Kumar, S. Ramalingam, C. Senthamarai, M. Niranjanaa, P. Vijayalakshmi and S. Sivanesan, *Desalin.*, **261**, 52 (2010).
34. S. Swain, T. Patnaik, V. Singh, U. Jha, R. Patel and R. Dey, *Chem. Eng. J.*, **171**, 1218 (2011).
35. A. A. Khan and R. P. Singh, *Colloids Surf.*, **24**, 33 (1987).
36. M. Jian, C. Tang and M. Liu, *Desalin. Water Treat.*, 1 (2014).
37. M. Naushad, *Chem. Eng. J.*, **235**, 100 (2014).
38. R. Bushra, M. Naushad, R. Adnan, Z. A. Alothman and M. Rafatullah, *J. Ind. Eng. Chem.*, **21**, 1112 (2015).
39. X. Liang, W. Hou, Y. Xu, G. Sun, L. Wang, Y. Sun and X. Qin, *Col-*

*loids Surf., A*, **366**, 50 (2010).
40. X. Liang, W. Hou and J. Xu, *Chin. J. Chem.*, **27**, 1981 (2009).
41. M. Ghasemi, M. Naushad, N. Ghasemi and Y. Khosravi-fard, *J. Ind. Eng. Chem.*, **20**, 2193 (2014).
42. J. Kong, Q. Yue, S. Sun, B. Gao, Y. Kan, Q. Li and Y. Wang, *Chem. Eng. J.*, **241**, 393 (2014).
43. F. Boudrahem, F. Aissani-Benissad and H. Aït-Amar, *J. Environ. Manage.*, **90**, 3031 (2009).
44. T. Gan and K. Wu, *Colloids Surf., A*, **330**, 91 (2008).
45. J. U. K. Oubagaranadin and Z. V. P. Murthy, *Ind. Eng. Chem. Res.*, **48**, 10627 (2009).
46. Y. Yasin, M. Mohamad, A. Saad, A. Sanusi and F. H. Ahmad, *Desalin. Water Treat.*, **52**, 4266 (2014).
47. R. Rojas Delgado, C. P. De Pauli, C. B. Carrasco and M. J. Avena, *Appl. Clay Sci.*, **40**, 27 (2008).